Energy Engineering

Tech Science Press

https://doi.org/10.32604/ee.2025.074947

ARTICLE

A Phased Active Frequency Support Strategy Tailored for Wind Power HVDC Transmission Systems

Guoqing Li, Jian Lou, Shouqi Jiang*, Yechun Xin, Yanxu Wang and Tuo Wang

The Key Laboratory of Modern Power System Simulation and Control & Renewable Energy Technology, Ministry of Education, Northeast Electric Power University, Jilin, 132012, China

*Corresponding Author: Shouqi Jiang. Email: m15043264368@163.com

Received: 22 October 2025; Accepted: 08 December 2025; Published: 12 November 2026

ABSTRACT: To mitigate the frequency stability challenges arising from insufficient system inertia and inadequate damping capacity, a phased active frequency support control strategy for the sending-end grid with collaborative participation of wind power and modular multilevel converter-based high-voltage direct current (MMC-HVDC) is proposed, which realizes flexible mutual support and efficient utilization of multiple frequency regulation units. For wind power, a macro-variable considering frequency and power deviations is constructed based on cooperative control theory, then an adaptive frequency cooperative control method is designed based on rotor speed and pitch angle adjustment, which realizes differentiated utilization of rotor kinetic energy while fully utilizing the power regulation capability of wind turbines. For MMC-HVDC, an active frequency support control method incorporating the effects of the regulation dead band is proposed, enabling adaptive switching of its frequency regulation performance according to the degree of disturbance. On this basis, a phased frequency coordinated control strategy considering the differences in frequency support characteristics of multi-type resources is proposed to maintain frequency stability while limiting the extent of disturbance influence, where the dead zone values of multi-type resources are designed based on their power regulation margins. Finally, the performance of the proposed control strategies is validated using real-time digital simulation.

KEYWORDS: Large-scale wind power; MMC-HVDC; phased frequency regulation control; dead zone; frequency active support

1 Introduction

Against the backdrop of the continuous large-scale development and widespread deployment of renewable energy, leveraging modular multilevel converter-based high-voltage direct current (MMC-HVDC) technology to efficiently collect and transmit power from large renewable energy bases has become a key trend in the future development of the energy sector [1–3].

The transmission of power from large-scale renewable energy bases via MMC-HVDC is generally characterized by weak connections to the sending-end AC grids [4], where the support from conventional power sources and the grid is limited, the system presents attributes such as diminished inertia, inadequate damping, and poor frequency regulation performance. As a result, frequency security and stability issues at the sending end are becoming increasingly critical [5,6]. Enabling wind power and MMC-HVDC to autonomously respond to grid frequency variations, and coordinating the utilization of the regulation

Copyright © 2027 The Authors. Published by Tech Science Press. This work is licensed under a Creative Commons Attribution 4.0 International License, which permits unrestricted use, distribution, and reproduction in any medium, provided the original work is properly cited.

capabilities of diverse frequency regulation resources within the sending-end system, are critical challenges that must be addressed to guarantee the secure and stable operation of the grid frequency.

To enable wind turbines to engage in the frequency regulation (FR) of the grid, the existing methods mainly consist of virtual inertia control, droop-based control, and load-shedding-based control methods. Reference [7] provides a comparative analysis of various auxiliary frequency regulation approaches in wind power applications, evaluating their respective strengths, limitations, and applicable scenarios, while also outlining future trends in wind power frequency support technologies. Reference [8] proposes an active power control strategy for doubly-fed induction generator (DFIG)-based wind turbines, using rotor-speed-based power increment, power attenuation trajectories, and parabolic compensation power to enable wind participation in frequency regulation, improving frequency nadir, eliminating overshoot, and mitigating secondary frequency dip. Reference [9] indicates that Dynamic Thermal Rating (DTR) technology, when accounting for frequency security constraints, helps mitigate transmission congestion, enhance system reliability under high wind power penetration, and supports renewable integration through strategies such as curtailment, synthetic inertia, de-loaded operation, and energy storage under varying load and penetration levels. Moreover, the combination of DTR with smart technologies such as Energy Storage Systems and network topology reconfiguration enables dynamic assessment of electrical equipment capacity, alleviating uncertainties and system stress caused by wind power integration, and providing practical measures for wind participation in frequency regulation [10]. Additionally, Reference [11] indicates that wind power forecasting and hybrid frequency control, including inertial and primary frequency control, are widely applied in high-penetration wind integration and are essential for ensuring future grid stability and reliability. Reference [12] proposes a frequency regulation method combining a three degree of freedom fractional order proportional integral derivative with model predictive control, using an intelligent optimization algorithm to tune controller parameters, effectively enhancing power system frequency stability and response under high load disturbances.

Control strategies for enhancing the frequency support capability of MMC-HVDC systems are mainly divided into two categories: grid-forming control and grid-following control. Among them, grid-forming control mostly adopts virtual synchronous control, which offers frequency assistance to the grid through mimicking the dynamic response of conventional synchronous generators [13,14]. Reference [15] combines the principle of virtual synchronous control to design a self-synchronization control strategy for the flexible DC system. The strategy enables the sending-end converter station to detect DC voltage variations in response to grid frequency changes, thereby achieving active inertia support. Reference [16] proposes an active power-DC voltage droop control based on virtual synchronization, which adjusts the droop coefficient according to the frequency margin to quickly regulate the output power of the converter station and suppress the rate of frequency change. Reference [17] proposes a self-synchronization control based on capacitor energy, which achieves decoupled control of the DC bus voltage and capacitor voltage, enabling rapid power support for the system. Grid-following control externally exhibits current-source characteristics, achieves synchronization with the system through a phase-locked loop (PLL), and mostly employs additional frequency control to provide frequency support to the system [18,19]. Reference [20] presents a microgrid wind power optimization approach integrating Dynamic Thermal Line Rating (DTLR) with electric vehicle scheduling, which dynamically adjusts transmission capacity and leverages EV storage, improving wind power utilization and reducing operational costs, providing guidance for wind power and DC/microgrid coordinated control. Reference [21] introduces a strategy for the coordinated utilization of DC capacitor energy and rotor kinetic energy of wind turbines, with successive action coordination, to actively assist in system frequency regulation. Reference [22] realizes active inertia support across multiple time scales by establishing the coupling relationship between grid frequency and inertia time constant. Reference [23]

proposes a frequency-priority selection control strategy for asynchronously interconnected grids, enabling fast active support for both sides based on support priorities. Reference [24] presents a communication-free control approach based on DC voltage/frequency droop control, employing the rotor kinetic energy of wind farms to deliver inertia support.

In summary, existing studies mainly focus on frequency active support control of single resources, lacking control methods that simultaneously consider system-level optimization and reliability coordination [25,26]. Under increasingly complex operating conditions, frequency stability and system reliability face new challenges. Therefore, it is necessary to fully tap the control potential of wind power, synchronous generators, and MMC-HVDC, and enhance frequency stability of the system through collaborative participation of multi-type resources.

Under this background, this paper proposes a phased active frequency support coordinated control method for the sending-end grid with collaborative participation of wind power and MMC-HVDC. The contributions mainly include three parts:

(1) For DFIG, by establishing a coupling among frequency deviation, power deviation, and rotor speed, an adaptive control law with rotor speed and pitch angle adjustment is designed to enhance frequency support through full use of power regulation and rotor kinetic energy.
(2) For MMC-HVDC, an active frequency support control method that explicitly considers the frequency regulation dead zone is proposed, so as to adaptively switch its frequency regulation performance according to the disturbance level, while preserving sending-end system frequency stability, the affected range of disturbances is reduced as much as possible.
(3) For multi-type frequency regulation resources, considering the frequency support requirements under different power disturbance scenarios and the power margin differences of various types of resources, a phased frequency regulation control strategy based on coordinated dead zone optimization is proposed, which enables optimized utilization and differentiated participation of diverse frequency regulation resources under varying disturbance conditions. Finally, the validity and performance of the proposed strategy are confirmed using a real-time digital simulation model.

2 The Configuration of Large-Scale Wind Power Transmission via MMC-HVDC

The structure and control scheme of the MMC-HVDC system are illustrated in Fig. 1. The sending-end system mainly consists of equivalent wind turbines, synchronous generators (SG), and local loads, while the receiving-end system is composed of loads and an equivalent infinite bus. Under conventional control, the sending-end MMC adopts active power and reactive power control to guarantee stable power transfer from the sending-end system, while the receiving-end MMC employs DC voltage and reactive power control to maintain DC voltage stability.

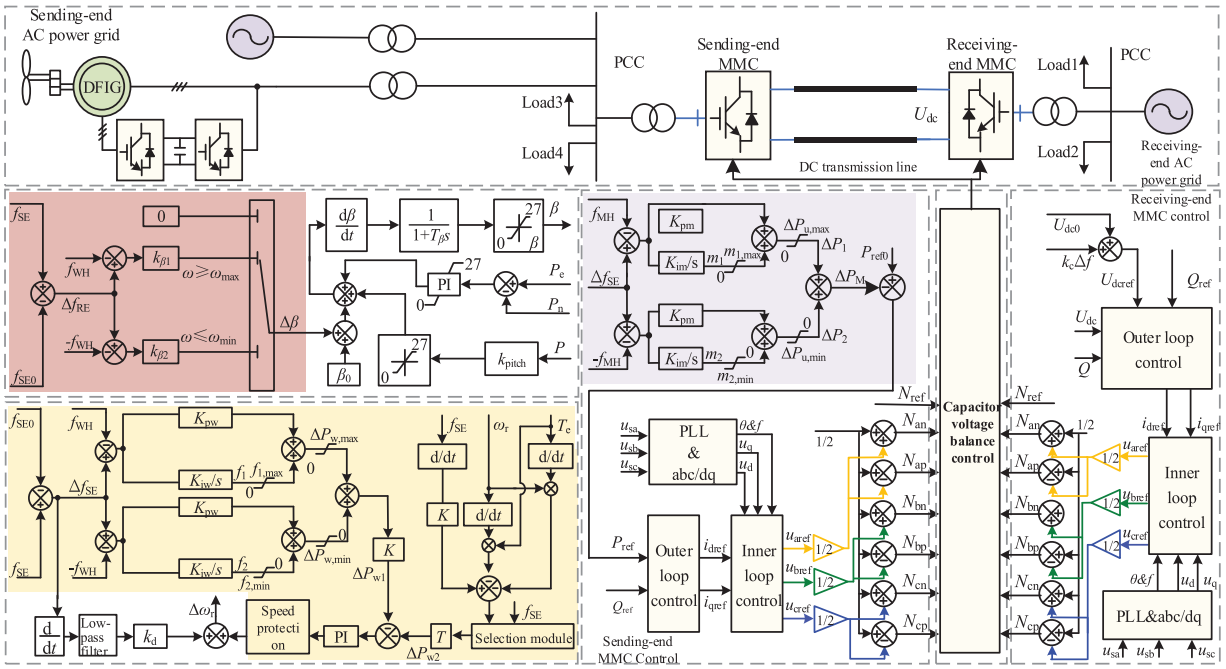


Figure 1: The structural and control block diagram of large-scale wind power transmission via MMC-HVDC

3 Frequency Regulation Control Methods for DFIG and MMC-HVDC

3.1 Active Frequency Support Control for DFIG Based on Cooperative Control Theory

The cooperative control theory adopts nonlinear models, which can achieve flexible mutual support and efficient coordinated utilization of resources within the system, enabling the system to rapidly transition from an unstable state to a stable state. For an n-dimensional nonlinear system $X\,\mathrm{cot} = f(x, u, t)$, according to the control objectives and performance requirements of the system, the macro-variable $\Psi(x)$ is constructed by using the linear combination of the state variables x. Based on the macro-variable constraint shown in (1), the system is made to gradually converge to the manifold $\Psi(x) = 0$. Solving Eq. (1) and substituting it into (2) allows the control law to be derived. Cooperative control not only ensures fast and smooth frequency response with high robustness, but also features a simple structure suitable for real-time implementation, and naturally coordinates multiple frequency-regulation resources along with staged dead-zone strategies, making it especially suitable for large-scale wind power transmission via MMC-HVDC system.

$$T\dot{\psi} + \psi = 0 \tag{1}$$

where T denotes the time constant of the control system.

$$\dot{\psi}(x) = \dot{x}\frac{\mathrm{d}\psi(x)}{\mathrm{d}x} \tag{2}$$

To enable the active frequency support effect of DFIG to adapt to the system frequency, a frequency auxiliary controller is constructed based on the principle of cooperative control, as shown in (3), where the macro-variable is the linear combination of the system frequency deviation and the variation in active power output of the DFIG.

$$\psi = K\left(f_{\mathrm{SE}} - f_{\mathrm{SE0}}\right) - \left(P_{\mathrm{e}} - P_{\mathrm{W,ref}}\right) \tag{3}$$

where f_{SE} and f_{SE0} are the actual and rated frequency, respectively. K is the control coefficient, P_e is the actual active power of the DFIG, and $P_{W,ref}$ is the power reference value during the DFIG frequency regulation process.

As observed, the deviation in sending-end grid frequency shows a direct positive relationship with the system frequency modulation performance. The greater the proportion of the system frequency deviation in $\Psi(x)$, the stronger the active frequency support capability of DFIG. Substituting (3) into (1) yields (4).

$$\begin{cases} \psi = TK\left(\dot{f}_{SE} - \dot{P}_e\right) + K\left(f_{SE} - f_{SE0}\right) - \left(P_e - P_{W,ref}\right) \\ P_e = T_e\omega_r \end{cases} \tag{4}$$

where ω_r represents the rotor speed of the DFIG.

The power reference value of the DFIG during active frequency support is given as:

$$P_{W,ref} = P_{W,ref0} + \Delta P \tag{5}$$

where $P_{W,ref0}$ is the power reference value during the steady-state operation of DFIG, ΔP is the variation of output power during the frequency support process of DFIG.

Substituting (5) into (4) gives:

$$T\left(K\dot{f}_{SE} - \dot{T}_e\omega_r - T_e\dot{\omega}_r\right) + K\left(f_{SE} - f_{SE0}\right) - \left(T_e\omega_r - P_{W,ref0} - \Delta P\right) = 0 \tag{6}$$

Combining the aforementioned control law solving method and considering the steady-state operation characteristics of DFIG, (6) is simplified to obtain the control law as shown in (7).

$$\Delta P = -K\left(f_{SE} - f_{SE0}\right) - T\left(K\dot{f}_{SE} - \dot{T}_e\omega_r - T_e\dot{\omega}_r\right) \tag{7}$$

The corresponding rotor speed variation $\Delta\omega_r$ can be obtained based on ΔP, by superimposing $\Delta\omega_r$ onto the speed control loop, the dynamic regulation of DFIG active power output can be achieved, which enables it to take an active role in supporting the frequency of the sending-end grid. Additionally, a rotor speed protection link as shown in (8) is incorporated into the frequency auxiliary controller to avoid the issue of rotor speed over-limit caused by excessive absorption or release of rotor kinetic energy in DFIG.

$$\Delta\omega_r = \begin{cases} 0, & \omega_r \le \omega_{r,min} \text{ or } \omega_r \ge \omega_{r,max} \\ \Delta P\left(K_{sp} + \frac{K_{si}}{s}\right), & \omega_{r,min} < \omega_r < \omega_{r,max} \end{cases} \tag{8}$$

where K_{sp} and K_{si} are the proportional and integral parameters, respectively, and $\omega_{r,max}$ and $\omega_{r,min}$ define the upper and lower rotor speed boundaries during DFIG operation.

As can be observed, the design of the control coefficient K enables the wind farm to adjust its participation in frequency regulation in real time according to its own operating conditions, rationally allocate its regulation power, and fully exploit frequency regulation capabilities without compromising the operational safety of wind turbines.

In addition, an improved pitch angle-based active frequency support control strategy, as shown in Fig. 1, is developed to fully exploit the frequency regulation potential of the DFIG. When the rotor speed of DFIG reaches its limit, it will be activated, while maintaining the rotor speed of DFIG constant, an additional pitch angle adjustment $\Delta\beta_1$ that exhibits a positive correlation with the system frequency deviation is superimposed on the basis of the initial reserve pitch angle β_0.

Taking into account the coupled relationship between the sending-end grid frequency deviation $\Delta f_{SE} = (f_{SE} - f_{SE0})$ and $\Delta\beta_1$ as shown in Fig. 1, when the grid frequency rises, the control coefficient $k_{\beta 1}$ is designed

by combining the maximum sending-end grid frequency deviation $\Delta f_{\mathrm{SE,max}}$ with the maximum pitch angle adjustment $\Delta\beta_{\max}$, as shown in (9). Similarly, the control coefficient $k_{\beta 2}$ for frequency drop is designed by combining $\Delta f_{\mathrm{SE,max}}$ and β_0.

$$\begin{cases} k_{\beta 1} = \dfrac{27-\beta_0}{\Delta f_{\mathrm{SE,max}}}, & \Delta f_{\mathrm{SE}} > 0 \\ k_{\beta 2} = \dfrac{\beta_0}{\Delta f_{\mathrm{SE,max}}}, & \Delta f_{\mathrm{SE}} \le 0 \end{cases} \tag{9}$$

It can be seen that the values of $k_{\beta 1}$ and $k_{\beta 2}$ can be adjusted according to the operating conditions of the sending-end grid and DFIG, enabling differentiated participation of each DFIG in the wind farm in frequency regulation.

3.2 Frequency Regulation Control Method for MMC-HVDC Accounting for Dead Zone Effects

Once a disturbance occurs in the system, to enable the sending-end MMC to actively respond to the grid frequency change, a power increment ΔP_{M} caused by the frequency variation can be added to its active power control loop, to realize the adaptive adjustment of the active power delivered by MMC-HVDC, effectively suppressing the frequency variation trend, as shown in (10) and Fig. 1.

$$\begin{cases} \Delta P_{\mathrm{M}} = k_{\mathrm{im}} \dfrac{\Delta f_{\mathrm{SE}} - f_{\mathrm{MH}}}{s} + k_{\mathrm{pm}} \left(\Delta f_{\mathrm{SE}} - f_{\mathrm{MH}}\right) \\ \Delta f_{\mathrm{SE}} = f_{\mathrm{SE}} - f_{\mathrm{SE0}} \end{cases} \tag{10}$$

where ΔP_{M} is the variation of active power reference value of the sending-end MMC, k_{pm} and k_{im} denote the proportional and integral gains.

Under this condition, the frequency regulation process of the sending-end grid satisfies the relationship shown in (11), considering the synergistic support capabilities of the SG, DFIG, and MMC-HVDC.

$$\begin{cases} 2H_{\mathrm{SE}} \dfrac{\mathrm{d}f_{\mathrm{SE}}}{\mathrm{d}t} = \Delta P - \Delta P_{\mathrm{L}} \\ \Delta P = \Delta P_{\mathrm{s}} + \Delta P_{\mathrm{M}} + \Delta P_{\mathrm{W}} \end{cases} \tag{11}$$

where H_{SE} is the equivalent inertia time constant of the sending-end grid, ΔP_{L} is the power disturbance magnitude, ΔP_{s}, ΔP_{W}, and ΔP_{M} are the active power variation of the SG, DFIG, and sending-end MMC.

4 Phased Frequency Coordinated Control Strategy of Multi-Type Resources

Due to the significant differences in the demand for system frequency support under different power disturbance conditions, during system frequency regulation, the dynamic response and control capacity of heterogeneous frequency regulation resources in the sending-end grid should be thoroughly considered. Following the principle of maintaining system frequency stability while minimizing the scope of disturbance impact, i.e., utilizing local resources such as synchronous generators and wind turbines to absorb unbalanced power as much as possible, and adjusting DC power export only when necessary. A phased frequency coordinated control strategy for multi-type frequency regulation resources is proposed, by appropriately designing the frequency regulation dead zone, multiple-type resources can adaptively switch their frequency-regulation roles under different disturbance conditions. The SG, DFIG, and sending-end MMC establish dynamic coordination across the various frequency-regulation stages, jointly suppressing frequency deviations and maintaining system stability by sharing the regulation burden in a staged manner. The overall control procedure is illustrated in Fig. 2.

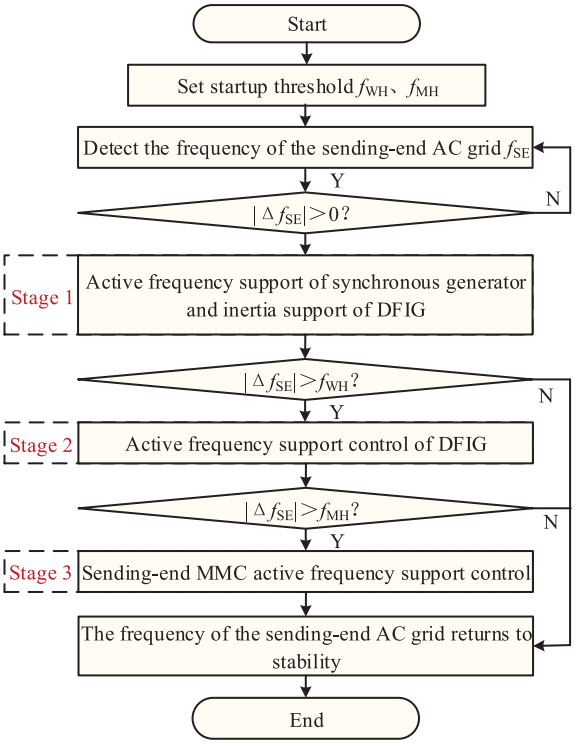


Figure 2: Phased frequency coordinated control strategy of multi-type resources

The detailed description of the frequency-regulation characteristics and interactions in each stage is as follows:

(1) Stage 1: When a power disturbance occurs, the frequency regulation task of the grid is first undertaken by SG. If the magnitude of the power disturbance is small, the inertia support provided by the DFIG, along with the frequency regulation capability of the synchronous generator, can effectively mitigate frequency variations in the sending-end grid. Once the system stabilizes at a new operating point, only the SG participates in the frequency regulation of the sending-end grid.

(2) Stage 2: If the power disturbance level is severe, and after the SG reaches its maximum power regulation margin, the system frequency deviation exceeds the designed dead zone f_{WH} of active frequency support control for DFIG. At this point, the disturbance power will be shared by both the DFIG and SG, entering the joint frequency regulation phase of synchronous generators and DFIG. Once the system stabilizes at a new operating point, the frequency deviation of the sending-end grid will be maintained at f_{WH}, with the power imbalance managed jointly by the DFIG and SG. Therefore, f_{WH} is determined based on the maximum active power regulation margin $\Delta P_{s,max}$ of the SG, as shown in (12).

$$f_{WH} = \Delta P_{s,max} \cdot \sigma \tag{12}$$

where σ is the primary frequency regulation coefficient of SG.

To achieve this control objective, an dead zone f_{WH}, a proportional-integral (PI) control link, and a selection module are introduced into the synergetic control-based DFIG active frequency support control. The control action principles are shown in (13) and (14), and the associated control schematic

is depicted in Fig. 1.

$$\begin{cases} \dfrac{\mathrm{d}f_{\mathrm{i}}}{\mathrm{d}t} = K_{\mathrm{iw}}\left(\Delta f_{\mathrm{SE}} - f_{\mathrm{WH}}\right) \\ \Delta P_{\mathrm{w1}} = -K\left[K_{\mathrm{pw}}\left(\Delta f_{\mathrm{SE}} - f_{\mathrm{WH}}\right) + f_{\mathrm{i}}\right] \end{cases} \tag{13}$$

$$\Delta P_{\mathrm{w2}} = \begin{cases} 0, & |\Delta f_{\mathrm{SE}}| < f_{\mathrm{WH}} \\ -T\left(K\dot{f}_{\mathrm{SE}} - \dot{T}_{\mathrm{e}}\omega_{\mathrm{r}} - T_{\mathrm{e}}\dot{\omega}_{\mathrm{r}}\right), & |\Delta f_{\mathrm{SE}}| < f_{\mathrm{WH}} \end{cases} \tag{14}$$

where f_{i} and $f_{\mathrm{i,max}}$ represent the DFIG state variables and their limiting values during the active frequency support process, K_{pw} and K_{iw} are the proportional and integral gains, ΔP_{w1} and ΔP_{w2} represent the additional power regulation amount of DFIG after the system frequency exceeds f_{WH}.

If the rotor speed of the DFIG reaches its limit in the process of regulating system frequency, the improved pitch angle-based DFIG active frequency support control described in Section 3 is activated. The additional pitch angle regulation amount is introduced into the pitch angle control to maximize its power regulation capability, as shown in (15).

$$\Delta\beta = \begin{cases} 0, & \omega_{\mathrm{r,min}} < \omega_{\mathrm{r}} < \omega_{\mathrm{r,max}} \\ K_{\beta 1}\left(\Delta f_{\mathrm{SE}} - f_{\mathrm{WH}}\right), & \Delta f_{\mathrm{SE}} > 0 \& \omega_{\mathrm{r}} = \omega_{\mathrm{r,max}} \\ K_{\beta 2}\left(\Delta f_{\mathrm{SE}} + f_{\mathrm{WH}}\right), & \Delta f_{\mathrm{SE}} < 0 \& \omega_{\mathrm{r}} = \omega_{\mathrm{r,min}} \end{cases} \tag{15}$$

where $\Delta\beta$ represents the variation of the DFIG pitch angle.

(3) Stage 3: If the power disturbance degree further increases, and the frequency deteriorates and exceeds the dead zone f_{MH} of the sending-end MMC active frequency support control, the sending-end MMC will adjust its injected power to maintain the frequency security and stability of the sending-end grid. At this point, both the SG and DFIG have reached their maximum power regulation margins, and the sending-end MMC takes full responsibility for the residual unbalanced power, entering the joint frequency regulation phase of SG, DFIG, and the sending-end MMC. When the system approaches steady state, the frequency deviation of the sending-end grid will be maintained at f_{MH}, so f_{MH} can be designed as:

$$\begin{cases} f_{\mathrm{MH}} = \Delta P_{\mathrm{m,max}}\sigma \\ \Delta P_{\mathrm{m,max}} = \Delta P_{\mathrm{s,max}} + \Delta P_{\mathrm{WF,max}} \end{cases} \tag{16}$$

where $\Delta P_{\mathrm{WF,max}}$ and $\Delta P_{\mathrm{m,max}}$ represents the upper limit of power regulation capability of the DFIG and the combined total power regulation margin together with SG.

At this time, the active power reference value of the sending-end MMC is:

$$P_{\mathrm{ref}} = P_{\mathrm{ref0}} + \Delta P_{\mathrm{M}} \tag{17}$$

where P_{ref0} and P_{ref} respectively represent the power reference values of the sending-end MMC before and after the activation of active frequency support control.

According to the analysis discussed above, the phased active frequency support control with collaboration between SG, DFIG and MMC-HVDC can realize differentiated participation of frequency support subjects according to the magnitude of system power disturbances. This control strategy exhibits superior frequency support performance while minimizing the impact range of power disturbances, thereby maintaining the frequency security and stability.

5 Simulation Verification

The MMC-HVDC-based large-scale wind power transmission system simulation model (as shown in Fig. 1) is built in Matlab/Simulink, and the Real-Time Laboratory (RT-LAB) real-time simulation platform is used for simulation. The detailed simulation parameters are listed in Table 1, respectively.

Table 1: Simulation parameters of the sending-end power grid

Simulation parameters	Value
Rated capacity of SG/MW	900
Droop coefficient of SG/p.u.	0.05
Rated capacity of DFIG/MW	900
Rated capacity of MMC-HVDC/MW	1500
$\Delta P_{m,max}$/MW	72
$\Delta P_{WF,max}$/MW	108
f_{WH}/p.u.	0.002
f_{MH}/p.u.	0.005

The simulations in this section are conducted under the conditions of Stage 1, Stage 2, and Stage 3 as outlined in Section 4, and sets up three simulation cases to verify the differences and advantages of the proposed method compared with typical control strategies in terms of multi-type frequency-regulation resource coordination, inertia support, frequency deviation suppression, and overall system stability. The detailed simulation scenarios are configured as follows:

Case 1: the DFIG only adopts the active frequency support control based on cooperative control (without virtual inertia control), and the sending-end MMC adopts active frequency support control.

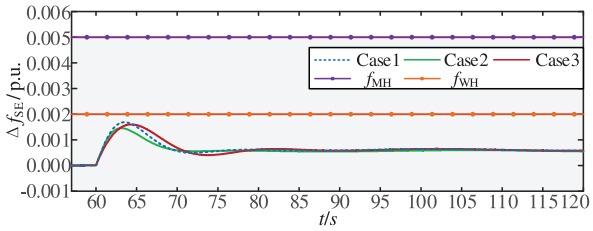
Case 2: the DFIG adopts virtual inertia control and droop control, and the sending-end MMC adopts *P/f* droop control, which are methods commonly used in practical engineering.

Case 3: adopt the proposed phased frequency coordinated control strategy of multi-type resources.

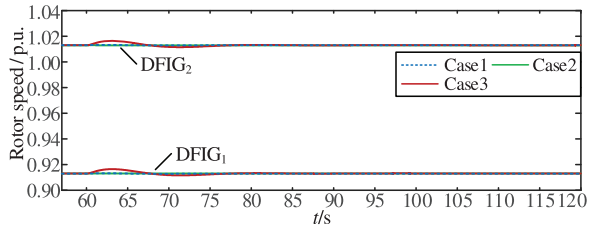
5.1 Stage 1 Simulation Verification

For Stage 1 verification after a power disturbance, the wind speeds of DFIG1 and DFIG2 are configured at 10 and 11 m/s to evaluate the control strategy's effectiveness. At t = 60 s, a simulation verification is conducted by removing a 30 MW load from the sending-end grid, and three simulation conditions (Case 1, Case 2, and Case 3) are set up. The results of the simulation are illustrated in Fig. 3.

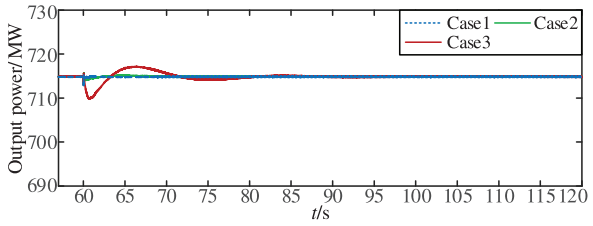
According to the simulation results, after load removal, the system frequency increases in Case 1, Case 2, and Case 3, as illustrated in Fig. 3a. In Case 3, the system frequency deviation does not exceed f_{WH}, and the designed phased frequency active support coordinated control strategy operates in Stage 1, where the unbalanced power is regulated by the joint participation of the DFIG and SG. During this process, the rotor speeds of DFIG1 and DFIG2 increase, reducing their output power to alleviate the frequency regulation burden on SG during the initial stage of power disturbance, thus effectively suppressing the frequency rise trend, as illustrated in Fig. 3b–d. During the frequency regulation process, the frequency deviation of the sending-end grid is maintained within f_{MH}, and the active power of the sending-end MMC remains constant. When the system tends to steady state, only the SG bear the unbalanced power, as illustrated in Fig. 3d,e. This verifies the effectiveness of the designed phased frequency active support coordinated control strategy in Stage 1.



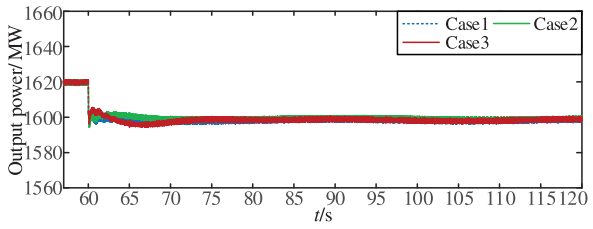
(**a**) Sending-end grid frequency deviation



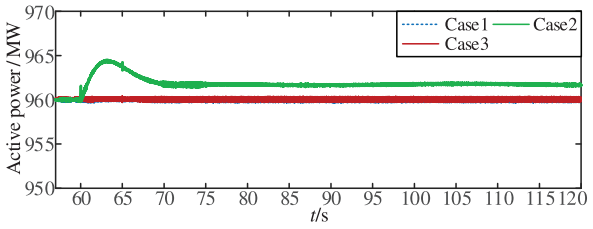
(**b**) Rotor speeds of DFIG$_1$ and DFIG$_2$



(**c**) Wind farm output power



(**d**) Output power of SG



(**e**) Active power of the sending-end MMC

Figure 3: Stage 1 simulation results

In Case 1, the dynamic characteristics of the sending-end grid frequency response are similar to those in Case 3, but the DFIG in Case 1 does not adopt virtual inertia control. Compared with Case 3, its inertia support capability during the initial stage of power disturbance is limited, so the initial rate of change of frequency is slightly higher, as shown in Fig. 3a.

In Case 2, which adopts *P*/*f* droop control, the sending-end MMC generates additional power regulation after power disturbance occurs, increasing its active power to suppress the frequency deviation, as illustrated in Fig. 3a,e. When the frequency tends to steady state, the unbalanced power is jointly borne by the sending-end MMC and SG, as illustrated in Fig. 3d,e. Compared with Case 2, Case 3 confines the disturbance impact

scope within the sending-end grid in the process of regulating system frequency. While rationally utilizing the frequency regulation capability of the sending-end grid to maintain frequency stability, it avoids system-wide power regulation caused by the expansion of power disturbance scope.

5.2 Stage 2 Simulation Verification

To assess the performance of the designed control strategy in Stage 2 after a power disturbance, the DFIG parameters are set the same as those in Stage 1, and a simulation verification is conducted by removing an 80 MW load from the sending-end grid at t = 60 s. The results of the simulation are illustrated in Fig. 4.

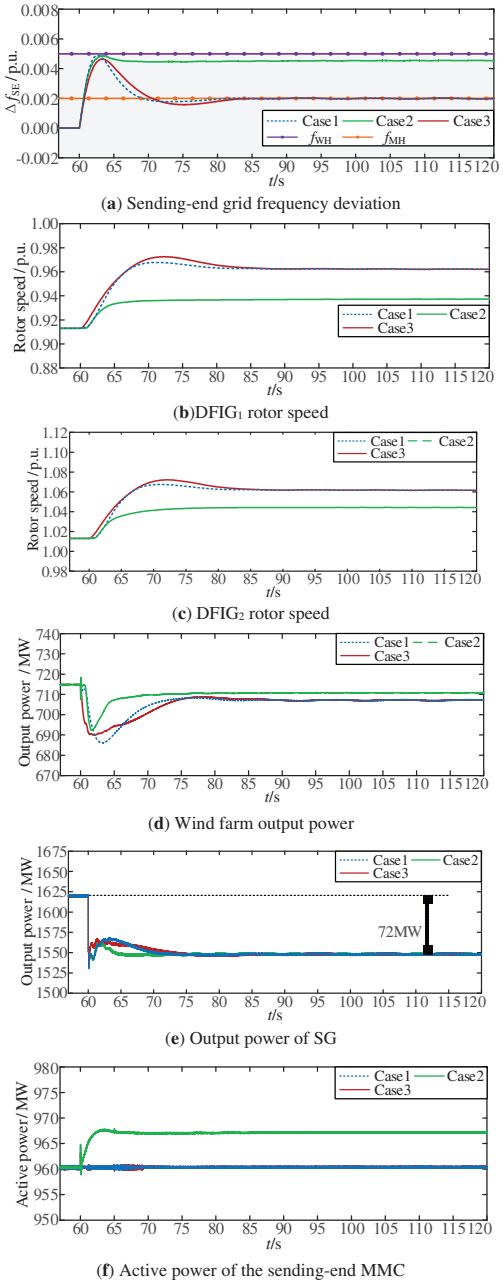


Figure 4: Stage 2 simulation results

According to the simulation results, after load removal, when the frequency deviation does not exceed f_{WH}, the dynamic behavior of active frequency support across Case 1, Case 2, and Case 3 is consistent with the earlier description. The difference is that when the power disturbance magnitude exceeds the $\Delta P_{m,max}$ of SG (72 MW), the frequency deviation in Case 3 exceeds f_{WH}, leading to the designed phased frequency active support coordinated control strategy operating in Stage 2. DFIG1 and DFIG2 quickly adjust their rotor speeds to absorb the remaining unbalanced power. When the sending-end grid tends to steady state, the unbalanced power is jointly borne by DFIG and synchronous generators, with the frequency deviation maintained at 0.002 p.u (f_{WH}), as shown in Fig. 4a–f. During this process, the maximum frequency deviation of the sending-end grid does not exceed f_{WH} of the sending-end MMC, and the active power reference value of the sending-end MMC remains constant. This verifies the effectiveness of the designed phased frequency active support coordinated control strategy in Stage 2.

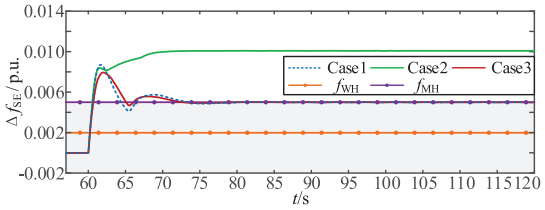
In comparison with Case 1 and Case 2, Case 3 fully exploits the DFIG's frequency regulation capability throughout the frequency adjustment process, achieving differentiated utilization of rotor kinetic energy while minimizing the impact scope of power disturbance and enhancing the frequency support performance.

5.3 Stage 3 Simulation Verification

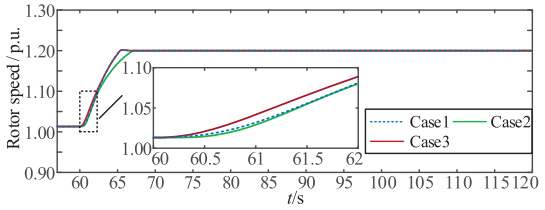
To assess the performance of the designed control strategy in Stage 3 after a power disturbance, a simulation verification is conducted where the wind speed of DFIG1 and DFIG2 are set to 10 m/s, and a 250 MW load is removed from the sending-end grid at t = 60 s. The results of the simulation are illustrated in Fig. 5.

The simulation results indicate that after the load is removed from the sending-end grid, the dynamic response processes of active frequency support in Case 1, Case 2, and Case 3 are consistent with the previous descriptions. The difference is that Case 3 maximizes the power regulation margin of SG while the rotor kinetic energy utilization margin of DFIG1 and DFIG2 reaches its adjustment upper limit under the active frequency support control based on coordinated control. At this point, the improved pitch angle-based DFIG active frequency support control is activated, generating an additional pitch angle adjustment to coordinate variable speed control and pitch control, thus fully exploiting the DFIG's frequency support capability, as shown in Fig. 5a–e. When the frequency regulation resources at the sending end, which provide up to 180 MW of adjustment capacity, cannot fully compensate for the power imbalance, causing the system frequency deviation to exceed f_{MH}, the designed phased frequency active support coordinated control strategy operates in Stage 3. The sending-end MMC active frequency support control is activated, proactively adjusting its active power to assume the remaining unbalanced power. When the sending-end grid moves toward a steady-state condition, the unbalanced power is distributed among the SG, DFIG, and the sending-end MMC, as shown in Fig. 5d–f. The validity of the designed coordinated control strategy for Stage 3 is demonstrated.

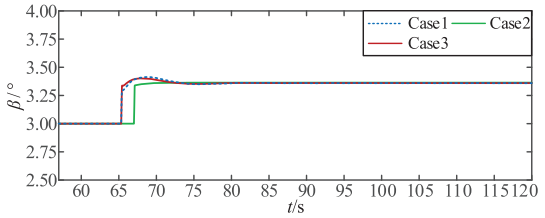
Compared with the results of Case 1 and Case 2, Case 3 maximizes the utilization of power regulation margins from multiple frequency regulation resources in the sending-end grid during frequency support, and achieves optimized utilization and collaborative complementarity of frequency regulation resources, resulting in a smaller frequency change rate and deviation at the initial stage of power disturbance, along with superior frequency dynamic regulation performance. However, in practical engineering applications, potential issues such as communication delays, measurement errors, and the operational safety of DFIG and MMC-HVDC under extreme conditions like high wind speeds or large power disturbances may affect the effectiveness of coordinated control of multi-type frequency-regulation resources, and should be carefully considered in system design and implementation.



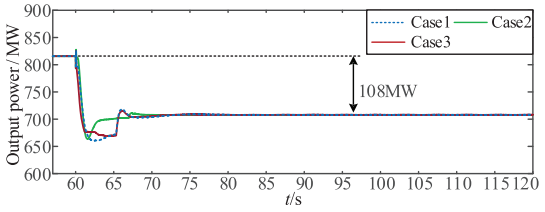
(a) Sending-end grid frequency deviation



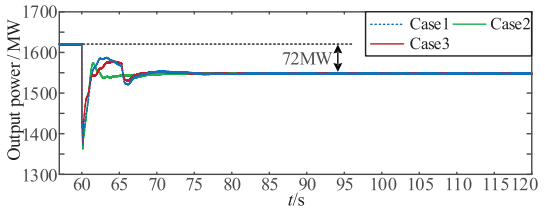
(b) DFIG$_1$ and DFIG$_2$ rotor speeds



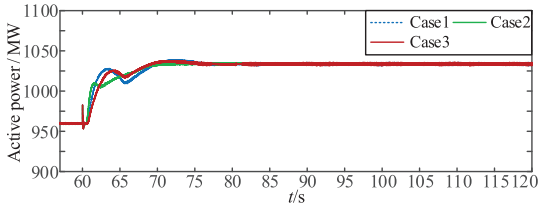
(c) DFIG$_1$ and DFIG$_2$ pitch angles



(d) Wind Farm output power



(e) Output power of SG



(f) Active power of the sending_end MMC

Figure 5: Stage 3 simulation results

6 Conclusion

To mitigate the frequency stability issues in the MMC-HVDC sending-end grid arising from the large-scale integration of renewable energy, this paper proposes a phased frequency support coordinated control strategy and dead zone design method, which enables flexible complementarity and efficient utilization of heterogeneous regulation resources within the region, thereby significantly enhancing the system's frequency support capability. Based on simulation analysis, the following conclusions can be obtained:

(1) For small power disturbances, the proposed strategy enables differentiated participation of local frequency-regulation resources according to the magnitude of the power disturbance, where DFIG has the capability to adaptively switch between providing inertia support and primary frequency regulation, fully utilizing the sending-end grid's capability to absorb unbalanced power while enhancing regional autonomy, and effectively mitigating the risk of frequency instability.

(2) For large power disturbances, through the coordinated design of dead-zone values for different frequency-regulation resources, they can adaptively switch their frequency-regulation roles according to the disturbance magnitude, while fully exploiting the control potential of MMC-HVDC, achieving wide-area coordinated and complementary operation of the MMC-HVDC interconnected system, and maintaining secure and stable system frequency.

Future work will explore the proposed method under more complex fault scenarios, integrate forecasting or artificial intelligence into cooperative control, and assess the effects of communication delays, measurement errors, and extreme conditions on heterogeneous frequency-regulation coordination, providing a basis for further theoretical refinement.

Acknowledgement: The authors would like to thank Northeast Electric Power University for its support of this study.

Funding Statement: This study is supported in part by the Smart Grid-National Science and Technology Major Project of China (No. 2024ZD0802700), and in part by the National Natural Science Foundation of China (Nos. 52207078 and 52577089).

Author Contributions: The authors affirm that their respective contributions to the manuscript are as follows: Guoqing Li: funding acquisition and methodology; Jian Lou: validation and original draft; Shouqi Jiang: conceptualization and analysis; Yechun Xin: project administration; Yanxu Wang: software; Tuo Wang: supervision. All authors reviewed the results and approved the final version of the manuscript.

Availability of Data and Materials: No data were generated or analyzed in this study.

Ethics Approval: Not applicable.

Conflicts of Interest: The authors declare no conflicts of interest to report regarding the present study.

References

1. Lu Y, Du Z, Li Y. Robust stability of grid-connected voltage source converter with phase-locked loop. IEEE Trans Power Syst. 2023;38(4):3981–4. doi:10.1109/tpwrs.2023.3273453.
2. Wang S, Shang L. Fault ride through strategy of virtual synchronous-controlled DFIG-based wind turbines under symmetrical grid faults. IEEE Trans Energy Convers. 2020;35(3):1360–71. doi:10.1109/tec.2020.2979885.
3. Lei J, Yang R, Wu W, Lu W, Mo W. Coordinated control strategy for HVDC frequency controllers in multi-area asynchronous grid. Int J Electr Power Energy Syst. 2025;167:110577. doi:10.1016/j.ijepes.2025.110577.
4. Sun K, Li KJ, Lee WJ, Wang ZD, Bao W, Liu Z, et al. VSC-MTDC system integrating offshore wind farms based optimal distribution method for financial improvement on wind producers. IEEE Trans Ind Appl. 2019;55(3):2232–40. doi:10.1109/tia.2019.2897672.

5. Shu H, Gao H, Shao Z, Cui Y, Zhao W. Research on primary frequency regulation and VSC-HVDC frequency synchronization control coordination method for large-scale hydropower DC export regional grid. Int J Electr Power Energy Syst. 2025;168:110655. doi:10.1016/j.ijepes.2025.110655.
6. Xiang W, Yang S, Adam GP, Zhang H, Zuo W, Wen J. DC fault protection algorithms of MMC-HVDC grids: fault analysis, methodologies, experimental validations, and future trends. IEEE Trans Power Electron. 2021;36(10):11245–64. doi:10.1109/tpel.2021.3071184.
7. Wang H, He H, Yang Z, Li G, Chen Z, Yang J, et al. Frequency response methods for grid-connected wind power generations: a review. Electr Power Syst Res. 2023;221:109396. doi:10.1016/j.epsr.2023.109396.
8. Zhao T, Liu H, Wang N, Su J, Luo Z, Ma S. An active power control of DFIG-based wind turbine generators for frequency regulation with expected dynamic performance. Appl Energy. 2025;391:125948. doi:10.1016/j.apenergy.2025.125948.
9. He X, Teh J, Alharbi B. Reliability impact of dynamic thermal rating on power system under high wind penetration and frequency security constraints. Appl Energy. 2025;400:126536. doi:10.1016/j.apenergy.2025.126536.
10. He X, Teh J. Impacts of dynamic thermal rating systems on wind generations: a review. Electr Power Syst Res. 2024;233:110492. doi:10.1016/j.epsr.2024.110492.
11. Loza B, Minchala LI, Ochoa-Correa D, Martinez S. Grid-friendly integration of wind energy: a review of power forecasting and frequency control techniques. Sustainability. 2024;16(21):9535. doi:10.3390/su16219535.
12. Gulzar MM, Sibtain D, Al-Dhaifallah M, Alismail F, Khalid M. A new optimal 3° of freedom fractional order proportion integral derivative controller with model predictive controller for frequency regulation in high penetrated renewable based interconnected system. Comput Electr Eng. 2024;119:109651. doi:10.1016/j.compeleceng.2024.109651.
13. D'Arco S, Suul JA. Virtual synchronous machines-classification of implementations and analysis of equivalence to droop controllers for microgrids. In: Proceedings of the 2013 IEEE Grenoble Conference; 2013 Jun 16–20; Grenoble, France. p. 1–7.
14. Zhang W, Cantarellas AM, Rocabert J, Luna A, Rodriguez P. Synchronous power controller with flexible droop characteristics for renewable power generation systems. IEEE Trans Sustain Energy. 2016;7(4):1572–82. doi:10.1109/tste.2016.2565059.
15. Yang R, Shi G, Cai X, Zhang C, Li G, Liang J. Autonomous synchronizing and frequency response control of multi-terminal DC systems with wind farm integration. IEEE Trans Sustain Energy. 2020;11(4):2504–14. doi:10.1109/tste.2020.2964145.
16. Wang R, Chen L, Zheng T, Mei S. VSG-based adaptive droop control for frequency and active power regulation in the MTDC system. CSEE J Power Energy Syst. 2017;3(3):260–8. doi:10.17775/cseejpes.2017.00040.
17. Yang R, Shi G, Zhang C, Li G, Cai X. Internal energy based grid-forming control for MMC-HVDC systems with wind farm integration. IEEE Trans Ind Appl. 2023;59(1):503–12. doi:10.1109/tia.2022.3205569.
18. Askarian A, Park J, Salapaka S. Enhanced grid-following (E-GFL) inverter: a unified control framework for stiff and weak grids. IEEE Trans Power Electron. 2024;39(5):5089–107. doi:10.1109/tpel.2024.3350528.
19. Lin H, Xue T, Lyu J, Cai X. Impact of different AC voltage control modes of wind-farm-side MMC on stability of MMC-HVDC with offshore wind farms. J Mod Power Syst Clean Energy. 2023;11(5):1687–99. doi:10.1049/icp.2021.2272.
20. Song T, Teh J. Coordinated integration of wind energy in microgrids: a dual strategy approach leveraging dynamic thermal line rating and electric vehicle scheduling. Sustain Energy Grids Netw. 2024;38:101299. doi:10.1016/j.segan.2024.101299.
21. Liu X, Xu Z. Coordinated frequency control scheme of offshore wind farm connected to VSC-HVDC. Electr Power Compon Syst. 2019;47(3):757–71. doi:10.1080/15325008.2019.1627602.
22. Shen Z, Zhu J, Ge L, Bu S, Zhao J, Chung CY, et al. Variable-inertia emulation control scheme for VSC-HVDC transmission systems. IEEE Trans Power Syst. 2022;37(1):629–39. doi:10.1109/tpwrs.2021.3088259.
23. Zhu J, Wang X, Zhao J, Yu L, Li S, Li Y, et al. Inertia emulation and fast frequency-droop control strategy of a point-to-point VSC-HVdc transmission system for asynchronous grid interconnection. IEEE Trans Power Electron. 2022;37(6):6530–43. doi:10.1109/tpel.2021.3139960.

24. Liu X, Lindemann A. Control of VSC-HVDC connected offshore windfarms for providing synthetic inertia. IEEE J Emerg Sel Top Power Electron. 2018;6(3):1407–17. doi:10.1109/jestpe.2017.2751541.
25. Zhang Z, Teh J. Enhancing grid flexibility and renewable integration: a review of V2G and dynamic line rating synergies. Renew Sustain Energy Rev. 2026;226:116341. doi:10.1016/j.rser.2025.116341.
26. Song T, Teh J, Alharbi B. Reliability impact of dynamic thermal line rating and electric vehicles on wind power integrated networks. Energy. 2024;313:133945. doi:10.1016/j.energy.2024.133945.